npj | breast cancer

Article

Published in partnership with the Breast Cancer Research Foundation

https://doi.org/10.1038/s41523-025-00889-7

# Agonistic CD40 elicits CD8+ T-cell-dependent primary responses and CD4+ T-cell-dependent long-term immunity in breast cancer



Casey Lam[1,4], Olivia Lanchoney[1,4], Vishnu Maddipatla[1], Nune Markosyan[2], Nikhil Joshi[1], Xiaowen Hu[3], Courtney Ray Fofana[2], Shan Zeng[1], Ronald P. DeMatteo[1], Robert H. Vonderheide[2] & Jennifer Q. Zhang[1,2] ✉

There has been marked improvement in the clinical outcome of triple-negative breast cancer (TNBC) with the use of immune checkpoint blockade (ICB) although serious immune-related adverse effects are not uncommon. However, other subtypes including luminal ER+ and HER2+ breast cancers are largely unresponsive to ICB. Approximately 35% of TNBCs also do not fully respond to ICB. Here we hypothesize that improving priming by cross-presenting conventional dendritic cells (cDCs) with an agonistic CD40 antibody (aCD40) may be complementary to ICB. Systemic administration of aCD40 induced T cell proliferation and activation in tumor-draining lymph nodes and attracted effector T cells to the tumor bed from the periphery. This effect was largely due to activation and maturation of type 1 conventional dendritic cells (cDC1s). aCD40 alone slowed tumor growth and its combination with ICB cured tumor-bearing mice, accomplishing a "vaccine effect" and the immune-mediated rejection of tumor rechallenge. The anti-tumor effect of aCD40 was cDC1 and CD8 + T cell-dependent, whereas the rejection of secondary tumor rechallenge in cured mice required CD4 + T cells. Importantly, intra-tumoral administration of aCD40 combined with systemic or intra-tumoral ICB—to mimic neoadjuvant therapeutic approaches—induced complete regressions of both treated and distant tumors. These findings demonstrate aCD40 efficacy in preclinical models of breast cancer and further supports intra-tumoral administration of both aCD40 and ICB as an effective treatment that might limit systemic exposure and lower risk of immune-related toxicity.

Breast cancer remains a leading cause of cancer-related mortality in women worldwide, with certain subgroups at higher risk of distant disease and death[1–3], highlighting the urgent need for alternative therapeutic approaches. Immune checkpoint blockade (ICB), which has revolutionized treatment paradigms across multiple cancer types, has demonstrated only modest efficacy in breast cancer, with anti-PD-1/PD-L1 and anti-CTLA4 monoclonal antibodies benefiting a small subset of patients with predominantly PD-L1-positive tumors[4–7]. ICB has demonstrated clinical efficacy in triple-negative breast cancer (TNBC)[8–10], improving the pathologic complete response (pCR) rates by 14% compared to traditional chemotherapy. However, ICB has limited efficacy in 35% of TNBC patients as well as in luminal estrogen receptor positive (ER+) and human epidermal growth factor receptor 2 (HER2) subtypes[11–14]. Breast cancers overall have relatively low density of tumor-infiltrating lymphocytes (TILs) and low tumor mutational burden (TMB)[15–17], suggesting an opportunity for immunotherapeutic strategies that can promote de novo T cell priming and enhance tumor T cell infiltration beyond checkpoint blockade alone. We thus pursued an alternative strategy via CD40 agonism to convert immunologically cold breast cancers into more highly inflammatory tumors capable of improved responsiveness to checkpoint blockade.

[1]Department of Surgery, University of Pennsylvania, Philadelphia, PA, USA. [2]Abramson Cancer Center, University of Pennsylvania, Philadelphia, PA, USA. [3]Department of Obstetrics and Gynecology, University of Pennsylvania, Philadelphia, PA, USA. [4]These authors contributed equally: Casey Lam, Olivia Lanchoney. ✉e-mail: Jennifer.zhang@pennmedicine.upenn.edu

CD40, a member of the tumor necrosis factor receptor superfamily expressed predominantly on antigen-presenting cells (APCs)[18], represents a promising immunotherapeutic target[19]. Activation of CD40 through agonistic antibodies initiates a cascade of immunological events critical for effective anti-tumor immunity[19]. Specifically, CD40 agonism promotes dendritic cell (DC) maturation, enhances antigen presentation, upregulates costimulatory molecules, and facilitates cross-presentation of tumor-associated antigens[20–25]. CD40 agonists have also demonstrated synergistic potential when administered with immune checkpoint inhibitors[26,27] and have been found to have acceptable safety profiles with evidence of clinical activity in human clinical trials[28–31]. Agonistic CD40 therapy has the potential to bridge the gap between innate and adaptive immunity by enabling robust CD8 + T cell priming and activation, potentially overcoming the immunosuppressive environment of breast cancers. Our present study evaluates the ability of aCD40 to improve anti-tumor immunity via DC activation and subsequent T cell priming and activation and to synergize with checkpoint blockade in murine breast cancer. Our findings suggest agonistic CD40 therapy may be a viable strategy for immune activation and long-lasting immunity in breast cancer.

## Results

### aCD40 suppresses tumor growth via cDC1 activity

A single dose of aCD40 suppresses tumor growth in multiple syngeneic orthotopic models of breast cancer including Brpkp110, E0771, AT3, and EpH4 1424 (Fig. 1A). Brpkp110, E0771, and AT3 models are on a B6 background, while EpH4 1424 is on a BALB/c background. In the Brpkp110 tumor model, aCD40 demonstrated the greatest tumor growth inhibition and achieved complete tumor regressions in 25% of mice (Fig. 1B). In vivo, Brpkp110 tumors express ERα by flow cytometry (Suppl. Fig. 1A) and IHC (Suppl. Fig. 1B) and are responsive to estradiol supplementation (Suppl. Fig. 1C), consistent with prior reports[32]. By gene expression, implanted Brpkp110 tumors demonstrate a mixed luminal ER-driven and basal phenotype (Suppl. Fig. 2A) based on PAM50-adapted subgroup classifications. Although Brpkp110 is an ERα + cell line, the level of ER expression in murine breast cancers may be lower compared to luminal human breast cancers given the substantially lower levels of ERα in luminal progenitor cells in mice compared to humans[33]. Consequently, it is challenging to apply the same "gold-standard" molecular classifications used in humans based on the PAM50 algorithm to our mouse models. We therefore adapted the PAM50 classification by analyzing its component gene signatures as separate functional subgroups (proliferation, basal, HER2-enriched, and luminal ER-related) to better capture the molecular heterogeneity of these models (Suppl. Fig. 2B). Similarly to previous reports[34], E0771 tumors have low ERα expression in vivo and are highly proliferative (Suppl. Fig. 2A), consistent with a luminal B subtype as reported previously[35]. AT3 and EpH4 1424 both exhibit a predominantly mixed HER2-enriched and basal phenotype (Suppl. Fig. 2). Agonistic CD40 suppresses tumor growth across murine models of varying molecular subtypes, including those with a luminal ER-driven signature and those with basal gene signatures.

We then focused on exploring the biologic effects of aCD40 in the Brpkp110 orthotopic model given its robust response. Tumor microenvironment (TME) analysis 7 days after a single dose of aCD40 revealed fewer EpCam+ tumor cells, a lower proportion of Ki67+ proliferating tumor cells, and increased tumor cell apoptosis by cleaved caspase 3 in treated tumors (Fig. 1C). These changes in the tumor cell population are unlikely to be a direct effect of aCD40 on tumor cells as only 1% of them expressed CD40 in vitro (Suppl. Fig. 3A). In contrast, about one-third of total cDCs, cDC1s, and cDC2s in untreated Brpkp110 tumors were CD40+ (Suppl. Fig. 3B). Seven days post aCD40 treatment, there were no changes in total cDC (Fig. 1D) and cDC2 populations (Fig. 1E) between control and treated tumors. However, cDC1 proportions within the tumor were lower in the aCD40 treated group (Fig. 1F). No increases in DC activation markers were seen within the tumor for either cDC1s or cDC2s (Suppl. Fig. 4). However, two days post-administration, aCD40 induced maturation and activation of cDC1s and cDC2s in the TDLN, with elevated expression of CD40, CD80, and CD86 (Figs. 1G and H, respectively). The time course of the changes in CD103+ migratory subpopulation of cDC1s showed that already on day 2 and 5 of aCD40 treatment, there was a significant decrease in the proportion of these cells in the tumor with a concomitant increase of the same cell population in tumor draining lymph node (TDLN) on days 5 and 7 (Fig. 1I). This is suggestive of a potential migration of a subset of cDC1s from the tumor into the TDLN after aCD40 treatment, although further studies are needed to test this hypothesis. There was a significant impact on tumor growth suppression with aCD40 when tumors were implanted into Batf3 knock out (KO) mice that lack cross-presenting cDC1s (Suppl. Fig. 5A and Fig. 1J), which illustrates the significant role of cDC1s in the anti-tumor effects of aCD40.

### aCD40 increases tumor-infiltrating cytotoxic T cells and exerts its anti-tumor effect via CD8 + T cells

On day 13 post-treatment, Brpkp110 tumors in mice treated with aCD40 had a higher percentage of CD3+ and CD8 + T cells and a trend towards a higher percentage of CD4 + T cells compared to the controls (Fig. 2A). In addition to an increase in activated CD8 + T cells, aCD40 treated tumors demonstrated decreased proportions of immunosuppressive CD4+ Foxp3+ regulatory T cells (Fig. 2B). CD4+ and CD8 + T cells appeared more activated in aCD40 treated tumors as the proportion of Granzyme B+ cells was higher in these populations (Fig. 2C). We confirmed the increase in CD8 + T cells in treated tumors by IF staining (Fig. 2D). In addition to increasing the number of tumor-infiltrating CD8 + T cells, aCD40 prompted their translocation from the tumor periphery to the center of the tumor (Fig. 2E). The increase in T cells in the TME after aCD40 treatment was possibly due to the increase in the production of chemokines such as CCL5, CCL21, CXCL9, and CXCL10 within the tumor (Fig. 2F). Within the TDLN, CD4+ and CD8+ cells were more activated after aCD40 treatment and exhibited higher Granzyme B expression and higher proportions of PD-1 and CD44 expressing cells (Fig. 2G). In addition, cell proliferation as measured by Ki67 was increased in CD4+ and CD8 + T cells after aCD40 treatment (Fig. 2G). To assess the dependency on T cells for the therapeutic effect of aCD40, tumor-bearing control and treated mice were depleted of CD8+ or CD4+ or both CD4+ and CD8 + T cells (Suppl. Fig. 5B). The tumor suppressive effect of aCD40 was abolished in the absence of CD8+ or CD8+ and CD4 + T cells (Fig. 2H, left and right). Although CD4 + T cells restrained the growth of control tumors, they were not necessary for the anti-tumor effect of aCD40 (Fig. 2H, middle). suggesting that aCD40 may be able to substitute for CD4+ help. Using FTY720, a S1P1 receptor antagonist[36], to block T cell egress from lymph nodes in the setting of aCD40, we observed a reduction in aCD40 efficacy in the presence of FTY720 (Fig. 2I). These data indicate that in addition to cDC1s, the aCD40 tumor-suppressive effect heavily relies on the presence and function of CD8+ cytotoxic T cells and partially on T cell migration from the TDLN.

### aCD40 enhances mammary tumor sensitivity to immune checkpoint blockade via cDC1s and both CD4+ and CD8 + T cells

The influx of T cells into the TME and their activation after aCD40 treatment inevitably leads to T cell exhaustion, potentially increasing sensitivity to ICB. We therefore hypothesized that combination with immune checkpoint blockade (ICB) would allow for further tumor suppression. Mice bearing Brpkp110 orthotopic tumors treated with aCD40 and ICB (αPD-1 and αCTLA-4) had smaller tumors and more complete tumor regressions, with a complete response rate up to 83%, than with either therapy alone (Fig. 3A). This is also seen in the luminal B E0771 model (Fig. 3B) and the mixed HER2-driven, basal, and luminal ER AT3 model (Fig. 3C). Mice bearing EpH4 1424 mixed HER2-driven and basal tumors demonstrated complete regressions with either ICB or combination aCD40 and ICB (Fig. 3D), with combination therapy resulting in more complete regressions at an earlier timepoint (15 days earlier) compared to either aCD40 or ICB alone (Suppl. Fig. 6). We then investigated the contribution of various immune subsets on the combination aCD40 and ICB therapeutic effect using Brpkp110 bearing

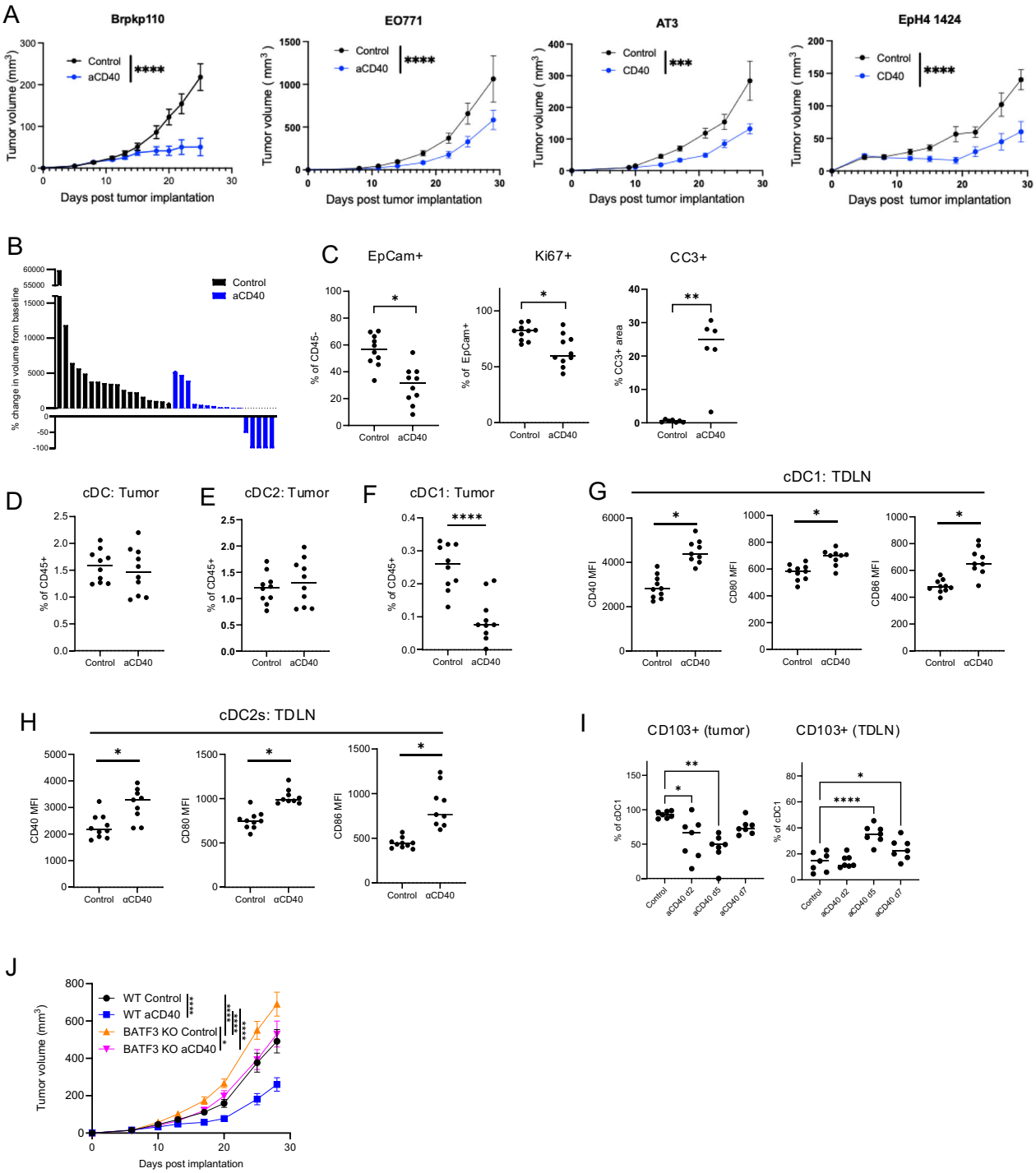


**Fig. 1 | aCD40 suppresses tumor growth via cDC1 activity. A** Growth curves of Brpkp110, E0771, AT3, and EpH4 1424 tumors after aCD40 or control treatments initiated on days 6, 8, 9, and 5, respectively ($n = 12–18$). **B** Tumor volume changes compared to pretreatment on day 25 post implantation of Brpkp110 tumor cells ($n = 16–18$). **C** Flow cytometry analysis of EpCam (left) and Ki67 (middle) expression in implanted control and aCD40 treated Brpkp110 tumors on day 7 post treatment ($n = 10$) and cleaved caspase 3 measured by IHC in control and aCD40 treated Brpkp110 tumors on day 5 post-treatment ($n = 6–7$). **D, E** DC proportions measured by flow cytometry in implanted control and aCD40 treated Brpkp110 tumors on day 7 post-treatment ($n = 10$). **F** cDC1 proportions measured by flow cytometry in implanted control and aCD40 treated Brpkp110 tumors on day 7 post-treatment ($n = 10$). **G** DC maturation and activation markers measured by flow cytometry in cDC1 cell populations of control and aCD40 treated Brpkp110 TDLN on day 2 post-treatment ($n = 8–10$). **H** DC maturation and activation markers measured by flow cytometry in cDC2 cell populations of control and aCD40 treated Brpkp110 TDLN on day 2 post-treatment ($n = 8–10$). **I** Proportions of CD103 + cDC1s measured in Brpkp110 tumors (left) and TDLN (right) on days 2, 5, and 7 post aCD40 administration, compared to untreated (control) tumors ($n = 6–7$). **J** Growth curves of control and aCD40 treated Brpkp110 tumors implanted into WT and BATF3 KO hosts ($n = 16–20$). Data: (**A**, **J**) mean ± SEM, (**B**) each column represents individual tumor, (**C–I**) median. $*p < 0.05$, $**p < 0.01$, $***p < 0.001$ and $****p < 0.0001$.

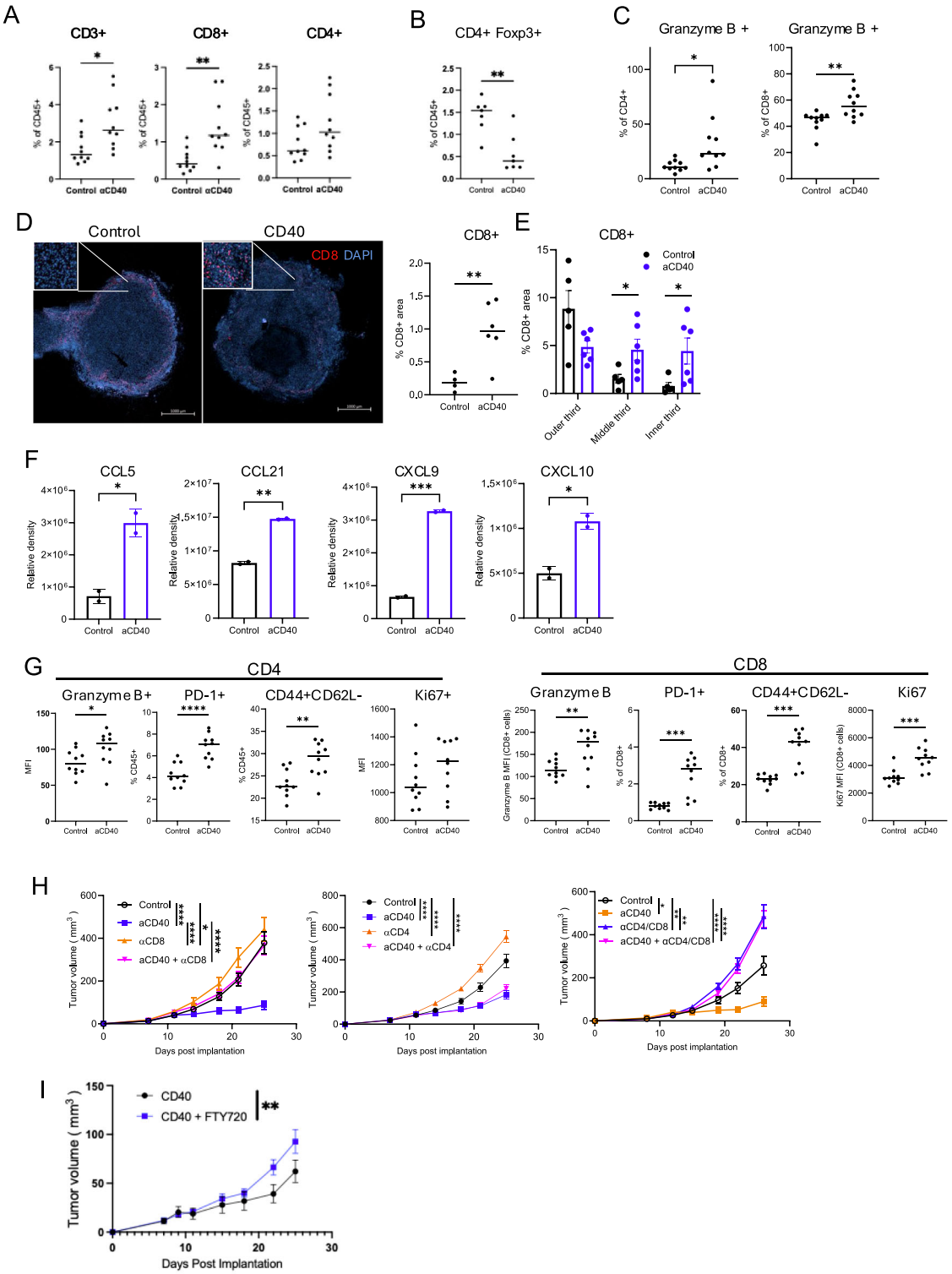


**Fig. 2 | aCD40 increases tumor-infiltrating cytotoxic T cells and exerts its anti-tumor effect via CD8 + T cells. A** Proportions of CD3+, CD8 +, and CD4 + T cells by flow cytometry in control and aCD40 treated Brpkp110 tumors on day 13 post treatment ($n = 10$). **B** FoxP3 + CD4+ regulatory T cells on day 7 post-treatment ($n = 7$). **C** Proportions of Granzyme B + T cells in subpopulations by flow cytometry in control and aCD40 treated Brpkp110 tumors on day 7 post implantation ($n = 10$). **D** Images of immunofluorescent staining for CD8 (red) and nuclei (blue) and CD8 staining quantification in untreated (control) and aCD40 treated Brpkp110 tumors on day 7 post treatment ($n = 4$–6). **E** Quantification of CD8 immunofluorescent staining in outer, middle, and inner thirds of control and aCD40 treated tumors on day 7 post treatment ($n = 5$–6). **F** After 7 days of treatment with aCD40, Brpkp110 tumors were minced and cultured ex vivo. Supernatant was collected and pooled for each treatment group after 48 h and cytokines were measured ($n = 2$, with 3 tumors pooled per group). **G** T cell activation and proliferation markers measured by flow cytometry in CD4+ and CD8 + T cell populations of control and aCD40 treated Brpkp110 TDLN on day 7 post-treatment ($n = 10$). **H** Growth curves of control and aCD40 treated Brpkp110 tumors implanted into WT hosts with or without T cell depletions ($n = 17$–20). **I** Tumor growth curve of aCD40 (treatment on Day 8) +/− FTY720 (treatment started on Day 7) treated Brpkp110 tumors ($n = 14$–16). Data: (**A**–**C**, **D** (right), **E**–**G**) median, (**H**, **I**) mean ± SEM. $^{*}p < 0.05$, $^{**}p < 0.01$, $^{***}p < 0.001$, and $^{****}p < 0.0001$.

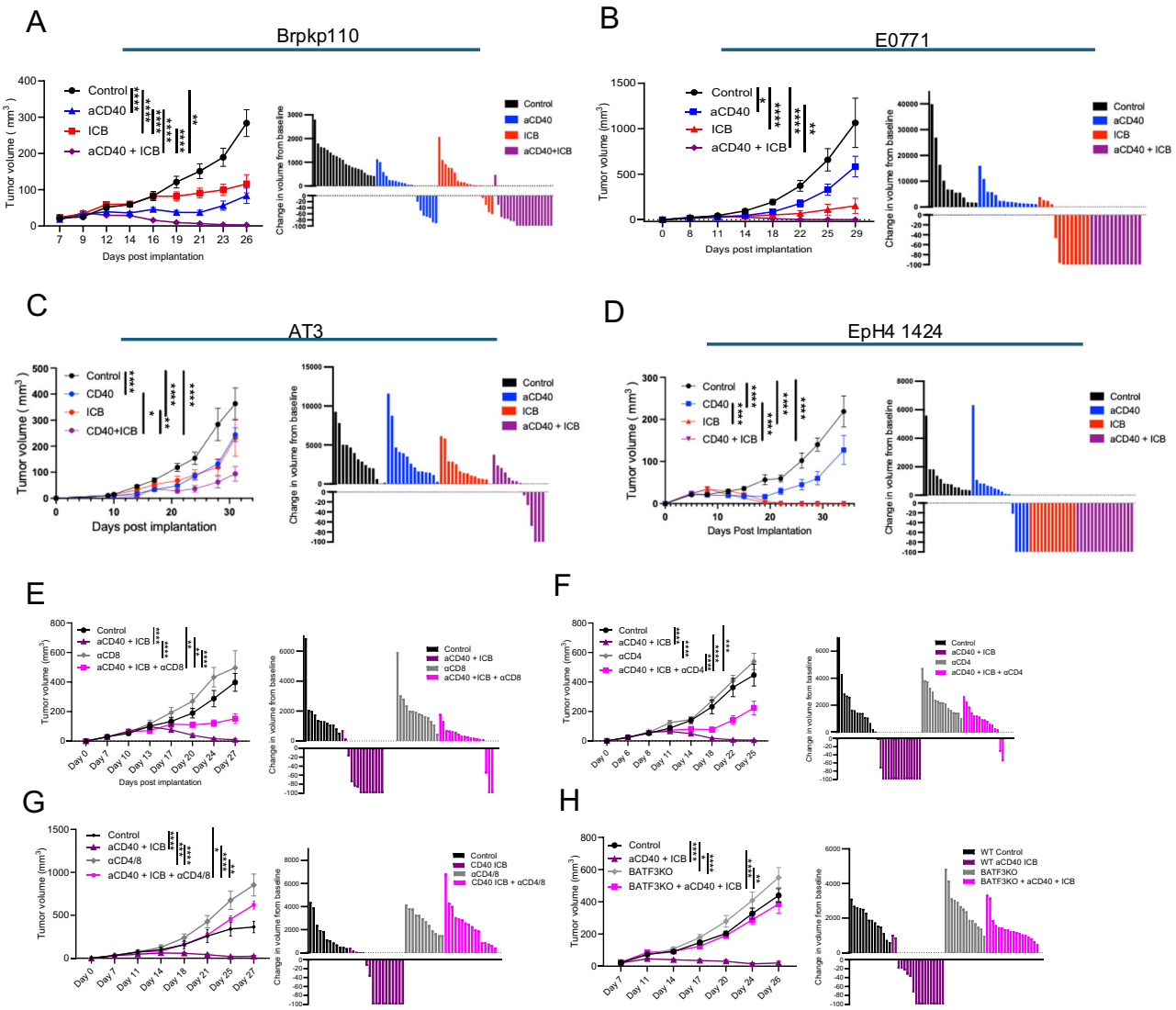


**Fig. 3 | aCD40 enhances mammary tumor sensitivity to immune checkpoint blockade via cDC1s and both CD4+ and CD8 + T cells. A** Tumor growth curves (left) and tumor volume changes compared to pretreatment on day 26 post implantation (right) of Brpkp110 tumors. Indicated treatments initiated on day 7 post implantation ($n = 18–20$). **B** Tumor growth curves (left) and tumor volume changes compared to pretreatment on day 26 post implantation (right) of E0771 tumors. Indicated treatments initiated on day 8 post implantation ($n = 12–15$). **C** Tumor growth curves (left) and tumor volume changes compared to pretreatment on day 31 post implantation (right) of AT3 tumors. Indicated treatments initiated on day 9 post implantation ($n = 14$). **D** Tumor growth curves (left) and tumor volume changes compared to pretreatment on day 34 post implantation (right) of EpH4 1424 tumors. Indicated treatments initiated on day 5 post implantation ($n = 14–16$). **E** Brpkp110 tumor growth curves (left) and volume changes compared to pre-treatment (right) on day 27 post implantation in control and aCD40+ICB treated hosts with and without CD8 + T cell depletions. Indicated treatments initiated on day 7 post implantation ($n = 12–15$). **F** Brpkp110 tumor growth curves (left) and volume changes compared to pretreatment (right) on day 25 post implantation in control and aCD40+ICB treated hosts with and without CD4 + T cell depletions. Indicated treatments initiated on day 8 post implantation ($n = 14–18$). **G** Brpkp110 tumor growth curves (left) and volume changes compared to pretreatment (right) on day 27 post implantation in control and aCD40+ICB treated hosts with and without CD4+ and CD8 + T cell depletions. Indicated treatments initiated on day 7 post implantation ($n = 12–18$). **H** Tumor growth curves (left) and volume changes compared to pretreatment (right) on day 26 post Brpkp110 tumor implantation into WT and BATF3 KO hosts. Indicated treatments initiated on day 7 post implantation ($n = 14–18$). Data: (**A**–**H** left) mean ± SEM, (**A**–**H** right) each column represents individual tumor. $^{*}p < 0.05$, $^{**}p < 0.01$, $^{***}p < 0.001$, and $^{****}p < 0.0001$.

mice. The effect of the combination therapy was only partially reversed by depletion of only CD8+ or CD4 + T cells (Fig. 3E and F, respectively), whereas combined CD8+ and CD4 + T cell depletion completely abolished the effect of aCD40+ICB treatment (Fig. 3G). Tumors implanted in Batf3 KO hosts were resistant to combination therapy (Fig. 3H).

### Combination aCD40 and ICB treatment results in a vaccine effect and allows for subsequent rejection of rechallenge tumors

The effect of combination immunotherapy on T cells persisted beyond the onset of tumor clearance. Two months after complete tumor regressions and cessation of treatment, the proportion of CD44 + CD62L- effector memory and CD44 + CD62L+ central memory CD4+ and CD8 + T cells were higher in the blood of cured mice compared to treatment-naïve mice implanted with tumors (Fig. 4A). At the same time, cured mice had fewer circulating CD44-CD62L- naïve T cells compared to treatment-naïve mice (Fig. 4A). The presence of effector and central memory T cells in cured mice is consistent with a vaccine effect and continued anti-tumor immuno-surveillance and immunologic memory. To test the robustness of this immunologic memory, cured mice were rechallenged with the same burden of Brpkp110 tumor cells. The cells grew in control, tumor naïve mice but were universally rejected in cured mice (Fig. 4B). The rejection of tumors upon secondary rechallenge was only CD4 + T cell-dependent and not

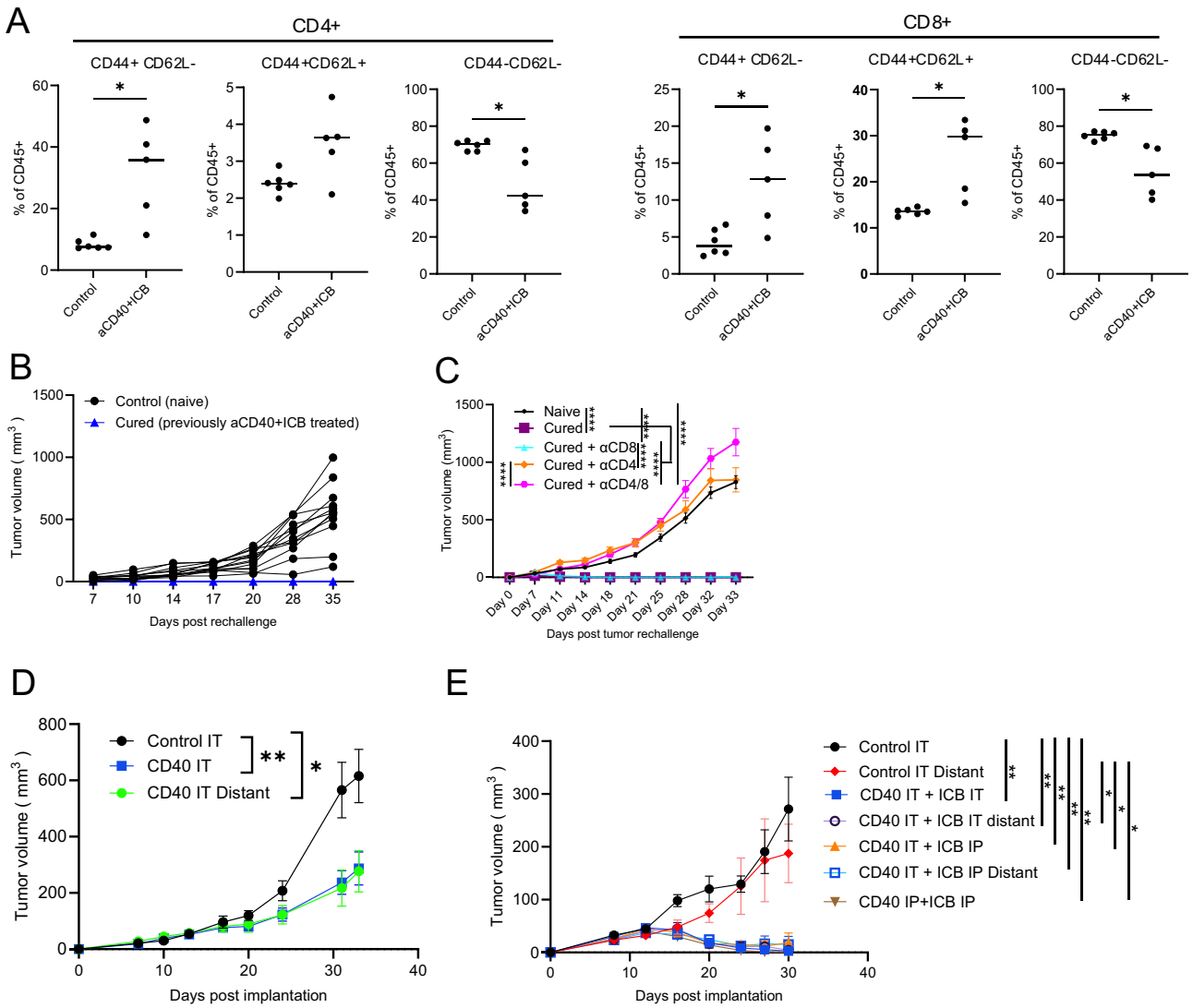


**Fig. 4 | aCD40 and ICB results in a vaccine effect and rejection of a secondary tumor rechallenge. A** Proportions of circulating effector memory (CD44 + CD62L-), central memory (CD44 + CD62L+), and naïve (CD44-CD62L-) CD4+ (left) and CD8+ (right) in blood, 3 months post treatment induced tumor clearance ($n = 5$–6, data representative of 2 experiments with similar results). **B** Secondary Brpkp110 tumor rechallenge of naïve and previously Brpkp110 tumor-bearing mice cured after aCD40 + ICB, at least 2 months post primary tumor clearance ($n = 12$–14, data representative of 3 experiments with similar results). **C** Control and rechallenge tumor growth in T cell sufficient ($n = 6$–12) and T cell depleted hosts ($n = 12$–14, data representative of 2 experiments with similar results). **D** Brpkp110 tumor growth curves in intra-tumoral (IT) vehicle (control) and IT aCD40 treated hosts. aCD40 administered tumors denoted as aCD40 IT and contralateral untreated tumors denoted as CD40 IT Distant ($n = 9$–12, data representative of 2 experiments with similar results). **E** Brpkp110 tumor growth curves in intra-tumoral (IT) vehicle (control) and IT or intraperitoneal (IP) aCD40 or ICB received hosts ($n = 4$–9, data representative of 2 experiments with similar results). Data: (**A**) median, (**C**–**E**) mean ± SEM. $^{*}p < 0.05$, $^{**}p < 0.01$, $^{***}p < 0.001$, and $^{****}p < 0.0001$.

CD8 + T cell-dependent, as the cured hosts depleted of only CD8 + T cells were able to reject a secondary tumor rechallenge similar to the cured, T cell sufficient hosts (Fig. 4C).

### Intratumoral administration of aCD40 + ICB suppresses the growth of treated and distant tumors

Intratumoral (IT) administration of ICB and aCD40 have individually been shown to be efficacious in human clinical trials without significant systemic absorption[37–39]. Here we tested the efficacy of IT aCD40 alone or in combination with IT ICB in double-flanked Brpkp110 tumor-bearing mice. IT aCD40 suppressed the growth of both the treated ipsilateral tumor as well as the distant contralateral tumor (Fig. 4D). Next, various combinations of IT and intraperitoneal (IP) administrations of aCD40 and ICB were tested in double-flanked hosts. IT aCD40 and ICB were able to suppress both the treated and distant tumors, similar to the effect observed in IP treatments (Fig. 4E), indicating that local administration of aCD40+ICB results in an abscopal effect on distant tumors.

## Discussion

In various immunologically "cold" tumor models, including pancreatic adenocarcinoma and glioblastoma, aCD40 has successfully activated cDC1s, improved T cell priming, and enhanced anti-tumor immunity[19,40]. We aimed to explore this strategy in breast cancers, which are relatively cold tumors due to their low TIL infiltration and TMB[15–17]. Immunotherapy in breast cancer has remained largely limited in scope, with pembrolizumab used only in the setting of a subset of TNBCs, The KEYNOTE-522 trial reported the addition of pembrolizumab to chemotherapy in high-risk early-stage TNBC led to an improvement in the pCR rate by 14%[41]. More recently, both nivolumab and pembrolizumab in combination with chemotherapy showed promising results in improving rates of pathologic

complete response (~24%)[41,42]. Therefore, additional strategies are needed to improve tumor response rates across breast cancer subtypes. We now show the first extensive characterization of the effect of aCD40 in multiple preclinical murine models of breast cancer, including models of different genetic backgrounds. This study demonstrates that agonistic CD40 antibody therapy enhances anti-tumor immunity in murine breast cancer models through cDC1-mediated T cell priming and activation, and synergizes with immune checkpoint blockade (ICB) to achieve durable complete responses and immunological memory. Surprisingly, when administered alone, the aCD40 therapeutic effect was mediated through CD8 + T cells only, while combination aCD40 and ICB treatment effect required both CD4+ and CD8 + T cells. In contrast, aCD40-induced immunological memory depended only on CD4 + T cells. Our findings provide several important insights into the mechanisms underlying CD40 agonism in breast cancer.

We have examined the efficacy of aCD40 monotherapy and aCD40 and ICB combination therapy across different molecular subtypes of breast cancer. The Brpkp110 model, which exhibits a mixed luminal ER-driven and basal phenotype, demonstrated the most robust response to aCD40 alone, with 25% complete regression rates. Although all models demonstrated increased tumor regression rates with aCD40 and ICB combination therapy, the greatest improvements in response rates with combination therapy were seen in the Brpkp110 and AT3 models, both of which are partially driven by the presence of ER signaling based on gene expression signatures. ICB alone had a robust response in the E0771 and AT3 models, which lack or have weak luminal ER gene signatures. It is important to note that murine luminal breast cancers may not perfectly recapitulate human luminal breast cancer biology, as luminal progenitor cells in mice express substantially lower levels of ERα compared to their human counterparts[33]. In addition, the majority of murine models of breast cancer are basal-like, with very few that are ER+ or mimic the luminal A subtype of most human breast cancers[43,44], making it difficult to extrapolate preclinical models to human biology. Classification according to human molecular subtypes can be ambiguous and inconsistent, with E0771 being a notable example. The E0771 cell line has been classified as triple-negative, luminal B-like, or ERα + luminal-like[34,35]. Molecular analyses of E0771 reveals the weak expression of ERα as well as its cytoplasmic location, as compared to the more robust ERα expression and nuclear localization in human breast cancers[34]. These inconsistencies highlight the importance of developing preclinical models which can recapitulate the ERα + luminal subtype seen in the majority of human breast cancers. Nevertheless, our data suggest that even tumors with partial ER+ luminal and HER2-driven signatures can be rendered more immunogenic through DC activation with aCD40.

Our observation that aCD40 treatment not only increased the number of tumor-infiltrating CD8 + T cells but also promoted their translocation from the tumor periphery to the center suggests that aCD40 remodels the tumor microenvironment to become more permissive to T cell infiltration and intratumoral trafficking. Following T cell priming in the TDLN, activated T cells must traffic back to the tumor to exert their effector functions. aCD40 treatment significantly increased tumoral expression of CCL5, potentially contributing to the recruitment of Granzyme B + CD4 + T cells from TDLNs to the tumor bed, as previously reported in pancreatic cancer models[45]. Concomitantly, we observed a marked reduction in Foxp3+ regulatory T cells within treated tumors, suggesting a shift in the CD4 + T cell population from an immunosuppressive to an immunostimulatory phenotype. Additionally, aCD40 enhanced tumoral production of CXCL9 and CXCL10, potent T cell chemoattractants that likely facilitated cytotoxic T cell trafficking to the tumor microenvironment[46]. Prior studies have demonstrated that the intratumoral activity of CXCR3 and its ligand CXCL9 are required for anti-PD-1 efficacy[47]. It is yet to be determined whether CXCL9/10 contribute to the anti-tumor effect of aCD40. However, we show that disruption of T cell trafficking from the TDLN does attenuate the therapeutic effect of aCD40. Following aCD40 administration, we observed increased DC activation markers specifically in the TDLN rather than within the tumor itself. The TDLN was also the first site of T cell activation at 2 days post aCD40 treatment, further supporting the concept that aCD40 enhances T cell priming in the lymph node microenvironment. We also observed a reduction in aCD40 efficacy with FTY720 treatment, which blocks lymphocyte egress from lymph nodes, indicating that T cell migration from the TDLN to the tumor is required for the full aCD40 anti-tumor effect.

Agonistic CD40 also induced upregulation of CCL21 within treated tumors. CCL21, traditionally produced by lymphatic endothelial cells and lymph node stromal cells, acts as a chemotactic signal for CCR7-expressing DCs to traffic to lymph nodes[48]. Beyond its role as a chemoattractant, CCL21 provides costimulatory signals that can enhance CD4+ and CD8+ naïve T cell expansion while promoting Th1 polarization, thereby preferentially activating effector immune responses[49], In preclinical breast cancer models, intratumoral administration of CCL21 has demonstrated therapeutic efficacy through enhanced recruitment of CD4+ and CD8 + T cells, NK cells, and dendritic cells to the tumor microenvironment, resulting in anti-tumor immunity. Further studies are needed to explore the role of tumor-associated CCL21 as well as the role of DC migration on the effect of aCD40 therapy.

Through selective depletion studies, we established that even though CD4 + T cells helps control baseline Brpkp110 tumor growth, initial therapeutic tumor regression following aCD40 monotherapy critically depends on CD8 + T cells but not CD4 + T cells, similar to prior data demonstrating that aCD40 can substitute for CD4 + T cell help[50]. The absence of Batf3-dependent cross-presenting cDC1s also abolished a significant proportion of the aCD40 anti-tumor effect, underscoring the essential role of cDC1s in initiating CD8 + T cell-mediated tumor immunity. Additional studies are needed to define the contributions of other cell types such as B cells and macrophages. In contrast, the efficacy of combined aCD40 and ICB treatment required both CD4+ and CD8 + T cells along with cDC1s for primary tumor rejection, suggesting that in the context of combination aCD40 and ICB, CD4 + T cells may provide additional effector functionality beyond their helper role in CD8 + T cell priming[51,52]. It also highlights the cooperative nature of these immune populations in mediating maximal therapeutic responses in the context of combination immunotherapy. The durable nature of the anti-tumor immunity was evidenced by elevated proportions of circulating effector and central memory T cells two months after tumor clearance, as well as the ability of cured mice to reject secondary tumor rechallenge, confirming the establishment of immunological memory via a vaccine effect. While primary tumor rejection required both CD4+ and CD8 + T cells, rechallenge tumor clearance demonstrated dependency on CD4 + T cells alone. This unexpected finding suggests that in the context of established immune memory, CD4 + T cells may either acquire direct cytotoxic functionality or orchestrate anti-tumor responses through cell populations other than CD8 + T cells. This observation warrants further investigation to delineate the precise mechanisms by which CD4 + T cells mediate tumor rejection in the memory phase.

Finally, our demonstration that intratumoral administration of aCD40, either alone or in combination with ICB, recapitulates the effects of systemic treatment has significant clinical implications. This finding indicates that localized immunomodulation within the primary tumor and associated TDLNs is sufficient to induce regression of distant lesions, potentially through the systemic dissemination of tumor-specific T cells. This approach could mitigate immune-related adverse events associated with systemic administration of immunotherapeutics, while maintaining therapeutic efficacy. Moreover, our data suggest that TDLNs play a crucial role in controlling distant metastatic lesions and preventing recurrence, arguing for the potential conservation of TDLNs during surgical resection to maximize the endogenous vaccine effect of the primary tumor. Our data support the clinical testing of IT administration in the neoadjuvant setting, where the primary tumor is still present and can serve as a source of tumor antigens, as a potentially effective way of inducing systemic anti-tumor immunity by transforming the tumor into an "in situ vaccine." A recent IT

aCD40 clinical trial in metastatic patients was well tolerated with one breast cancer patient experiencing a complete response[53].

In summary, we found that agonistic CD40 antibody therapy promotes cDC1-mediated T cell priming and activation, suppresses tumor growth across multiple molecular subtypes of breast cancer, and synergizes with ICB to achieve high rates of complete tumor regression and durable immunological memory. The differential requirements for CD4 + T cells in primary therapy versus memory responses highlight the complexity of aCD40 and ICB induced anti-tumor immunity. The demonstration that intratumoral administration can achieve systemic anti-tumor immunity provides a strong rationale for clinical translation of this approach as a method of limiting systemic immunotherapy-related toxicity. These findings support the development of DC-activating strategies combined with ICB as a promising therapeutic approach for breast cancer, including subtypes currently unresponsive to immunotherapy alone. This approach may dramatically expand the proportion of breast cancer patients who can benefit from immunotherapy, potentially addressing a critical unmet need. Furthermore, the mechanistic insights gleaned from this study may inform combination immunotherapy strategies across other immunologically "cold" tumor types characterized by deficient T cell priming and recruitment.

## Methods

### Cell lines

Brpkp110 is an estrogen receptor positive (ER+), progesterone receptor positive (PR+) and human epidermal growth receptor 2 negative (HER2-) mammary cell line derived from a tumor induced in the mammary gland of a *KRas*$^{G12D\text{-}LSL/wt}$;*p53*$^{flx/flx}$;*myr-p110α*$^{wt/fl}$ mouse (gift from Jose Conejo-Garcia, Duke University) which leads to constitutively activated PI3K signaling[32]. Brpkp110 cells were cultured in RPMI 1640 medium containing 10% fetal bovine serum, 1% penicillin/streptomycin, 0.05% sodium pyruvate, and 3.3 µL 2-mercaptoethanol. E0771 is a widely-used ERα- luminal B cell line[34,35] and was cultured in DMEM, 10% FBS, 1% glutamine, and 0.2% gentamicin. The AT3 murine mammary carcinoma cell line (Sigma-Aldrich SCC178) has been previously characterized as a basal-like cell line[54,55] but does have a low level of Erα expression[54], and were cultured in DMEM 10% FBS, 2mM L-glutamine, 1 mM sodium pyruvate, 2 mM non-essential amino acids, and 15 mM HEPES. The EpH4 1424 murine breast cancer cell line (ATCC CRL-3071) was cultured in high glucose DMEM, 10% FBS, and 200 µg/mL gentamicin. EpH4 1424 is derived from the EpH4 parental line which has been stably transfected with an expression vector containing Glu-Glu epitope-tagged phosphorylation site MEK1 mutant leading to constitutive MEK1 activation. Although the parental EpH4 mammary epithelial cell line demonstrates ERα and ERβ positivity[56], the EpH4 1424 cell line is not well characterized.

### Mice and treatments

Age- and sex-matched 7- to 18-week-old C57BL/6 mice (Jackson Laboratory, cat# 00664) and B6.129S(C)-*Batf3*$^{tm1Kmm}$/J (Jackson Laboratory, cat# 013755) were housed in specific pathogen-free conditions and treated as per an approved Institutional Animal Care and Use Committee protocol at the University of Pennsylvania (Protocol #804666). Tumors in C57BL/6 and B6.129S(C)-*Batf3*$^{tm1Kmm}$/J mice were established orthotopically in paired bilateral abdominal mammary glands 9 and 4 via injection of 5e5 cells of Brpkp110, E0771, AT3 cell lines. Tumors in BALB/cJ mice were established orthotopically in paired bilateral abdominal mammary glands 9 and 4 via injection of 1e6 cells of the EpH4 1424 cell line. The treatment antibodies listed below were obtained from Bio X Cell unless otherwise indicated. Tumor-bearing C57BL/6 or B6.129S(C)-*Batf3*$^{tm1Kmm}$/J mice received one dose of an agonistic CD40 antibody (clone FGK4.5, 100 µg intraperitoneal (i.p.) or intratumoral (i.t.)) or rat IgG2a (clone 2A3, 100 µg i.p. or i.t.) on day 0 as previously described[26]. Anti-CTLA-4 (clone 9H10, 200 µg i.p. or i.t.) or polyclonal Syrian hamster IgG (200 µg i.p. or i.t.) were given on day 0, 4, 7[26]. Anti-PD-1 (clone RMPI-14, 200 µg i.p. or i.t.) or rat IgG2b (clone LTF-2, 200 µg i.p. or i.t.) were given on day 0 and every 3 to 4 days thereafter[26]. Anti-CD4 (clone GK1.5, 200 µg i.p.) or rat IgG2b (clone LTF-2, 200 µg i.p.) was given on day −4, day 0, and every 3 to 4 days thereafter for CD4 T-cell depletion. Anti-CD8 (clone 2.43, 200 µg i.p.) or rat IgG2b (clone LTF-2, 200 µg i.p.) was given on day −4, day 0, and every 3 to 4 days thereafter for CD8 T-cell depletion. FTY720 (Selleckchem S5002) was administered starting 1 day prior to aCD40 treatment at 5 mg/kg i.p. daily.

### Tissue processing and flow cytometry

Mice were sacrificed according to IACUC approved protocols and tumors and tumor-draining lymph nodes (TDLN) were collected. Tumors were digested in 1 mg/mL collagenase with protease inhibitor (MilliporeSigma) and filtered through a 70 µm cell filter. TDLNs were mechanically dissociated and filtered using 100 µm filters. Cells were resuspended in PBS and incubated in Fc block (Biolegend 3527448) for 5 min on ice prior to staining for flow cytometry. The live/dead stain Zombie UV was used. Cells were stained with Zombie UV live/dead stain and for cell surface markers at 4 °C in the dark for 30 min. Cell suspensions were then fixed and permeabilized for 30 min (eBioscience Intracellular Fixation & Permeabilization Buffer Set, Invitrogen) and overnight staining was performed for intracellular targets. Conjugated antibodies used for flow cytometry were obtained from BD Biosciences [PD-L1 (clone MIH5), CD4 (clones GK1.5, RM4-5), CD103 (clone M290), CD80 (clone 16-10A1), FoxP3 (clone R16-715)], Biolegend [EpCam (clone G8.8), CD45 (clone 30-F11), Ki67 (clone 16A8), Granzyme B (clone AQA16A02), CD8 (clone 53-6.7), CD3 (clone 145-2C11), CD40 (clone 3/23), CD86 (clone G2-1), PD-1 (clone 29F.1A12), CD19 (clone 6D5), B220 (clone RA3-6B2), CD11c (clone N418), NK1.1 (clone PK136), Gr-1 (clone RB6-8C5), XCR1 (clone ZET), CD11b (clone M1/70), CD64 (clone X54-5/7.1), SIRPα (clone P84), CD44 (clone IM7), CD62L (clone MEL-14)], and Abcam [ERα (clone E115). Flow cytometry was performed using an LSRFortessa or FACSymphony A3 Cell Analyzer and data were analyzed using FlowJo v10.8 software (BD Biosciences).

### Immunohistochemistry and immunofluorescence

Tumor tissues were fixed in Zinc formalin for 24 h and embedded in paraffin. Immunohistochemistry (IHC) for ERα + (clone E115, Abcam 32063, 1:9000) and cleaved caspase-3 (Cell Signaling Technology 9661, 1:500) was performed by the Comparative Pathology Core of the University of Pennsylvania School of Veterinary Medicine. Immunofluoresence (IF) for CD8 and DAPI (Thermo Scientific D21490, 1:1000) was performed according to the Immunofluorescent Staining of Paraffin-embedded Tissue Protocol from Novus Biologicals, with certain modifications as follows. Antigen retrieval was performed using the IHC-Tek Epitope Retrieval Solution (IHC World 1W-1100), with slides incubated for 45 min in an IHC World steamer at 95–98 °C. Tissue sections were blocked with 5% donkey serum diluted in PBS with 0.3% Triton X-100 and stained with rabbit anti-mouse primary CD8 (clone: D4W2Z, Cell Signaling Technology 98941, 1:100) followed by donkey anti-rabbit Alexa Fluor 594 (Thermo Scientific A-21207, 1:250) secondary antibody. Slide scanning was performed on Aperio Versa 8 slide scanner at the Molecular Pathology and Imaging Core facility at the University of Pennsylvania. Data were analyzed using QuPath. In short, QuPath's wand function was utilized to draw a border around the DAPI-stained tissue area. Then, the "Thresholder" function was utilized to gate for positive antibody-staining, in both IF and IHC, which could be visualized in real-time. Once an appropriate staining threshold value was determined for positive-staining gating it was applied to whole tissue sections. QuPath quantified percent positive area for each antibody was used for analysis.

### Cytokine analysis

Brpkp110 tumor-bearing mice underwent treatment as described in results. Mice were euthanized and tumors were collected at day 7 post treatment. Tumors were minced and incubated in media for 48 h. Supernatant was collected and pooled per treatment group and cytokine array was performed

with technical duplicates via the proteome profiler (R&D, catalog # ARY028).

### Bulk RNA sequencing

Brpkp110, E0771, AT3, and EpH4 1424 orthotopic tumors were harvested from mice ($n = 4$ per group) and total RNA was extracted for RNA sequencing (Qiagen). Poly(A)-enriched sequencing libraries were prepared and sequenced on an Illumina NextSeq 2000 platform to generate paired-end reads. Sequencing reads were quality-checked with FastQC and aligned to the mouse reference genome (GRCm39) using STAR aligner. Gene-level counts were calculated by HTSeq. Mouse genes adapted from the PAM50 gene signature were assigned to four functional groups according to their molecular roles. For each group we computed a per sample signature score using ZMAD-normalized expression (modified Z-score based on the mean absolute deviation). Selected marker FPKM values were first log-transformed ($\log_2(\text{FPKM} + 0.01)$), then normalized using the ZMAD procedure. The signature score for a given sample and group is the mean of the ZMAD values for all genes in that group.

### Statistical analysis

Tumor growth curves were analyzed using two-way ANOVA with Tukey multiple comparisons of means to compare differences between two individual groups. A two-tailed Student $t$ test was used to analyze differences between two groups. One-way ANOVA with the Bonferonni multiple comparison test was used to assess differences between any two individual groups. Statistical analyses were performed using GraphPad Prism 10. $P \leq 0.05$ was considered statistically significant.

## Data availability

The datasets generated and/or analyzed during the current study are available in the Sequence Read Archive (SRA) repository accession code SUB15367120.

Received: 4 June 2025; Accepted: 31 December 2025;
Published online: 13 January 2026

## References

1. Siegel, R. L., Giaquinto, A. N. & Jemal, A. Cancer statistics, 2024. *CA Cancer J. Clin.* **74**, 12–49 (2024).
2. Howlader, N. et al. US incidence of breast cancer subtypes defined by joint hormone receptor and HER2 status. *J. Natl Cancer Inst.* **106**, dju055 (2014).
3. Pan, H. et al. 20-Year risks of breast-cancer recurrence after stopping endocrine therapy at 5 years. *N. Engl. J. Med.* **377**, 1836–1846 (2017).
4. Adams, S. et al. Current landscape of immunotherapy in breast cancer: a review. *JAMA Oncol.* **5**, 1205 (2019).
5. Cortes, J. et al. Pembrolizumab plus chemotherapy in advanced triple-negative breast cancer. *N. Engl. J. Med.* **387**, 217–226 (2022).
6. Schmid, P. et al. Atezolizumab and Nab-paclitaxel in advanced triple-negative breast cancer. *N. Engl. J. Med.* **379**, 2108–2121 (2018).
7. Schmid, P. et al. Overall survival with pembrolizumab in early-stage triple-negative breast cancer. *N. Engl. J. Med.* **391**, 1981–1991 (2024).
8. Schmid, P. et al. Atezolizumab plus nab-paclitaxel as first-line treatment for unresectable, locally advanced or metastatic triple-negative breast cancer (IMpassion130): updated efficacy results from a randomised, double-blind, placebo-controlled, phase 3 trial. *Lancet Oncol.* **21**, 44–59 (2020).
9. Cortes, J. et al. Pembrolizumab plus chemotherapy versus placebo plus chemotherapy for previously untreated locally recurrent inoperable or metastatic triple-negative breast cancer (KEYNOTE-355): a randomised, placebo-controlled, double-blind, phase 3 clinical trial. *Lancet* **396**, 1817–1828 (2020).
10. Schmid, P. et al. Pembrolizumab for early triple-negative breast cancer. *N. Engl. J. Med.* **382**, 810–821 (2020).
11. Dirix, L. Y. et al. Avelumab, an anti-PD-L1 antibody, in patients with locally advanced or metastatic breast cancer: a phase 1b JAVELIN Solid Tumor study. *Breast Cancer Res. Treat.* **167**, 671–686 (2018).
12. Rugo, H. S. et al. Safety and antitumor activity of pembrolizumab in patients with estrogen receptor-positive/human epidermal growth factor receptor 2-negative advanced breast cancer. *Clin. Cancer Res.* **24**, 2804–2811 (2018).
13. Loi, S. et al. International Breast Cancer Study Group and the Breast International Group. Pembrolizumab plus trastuzumab in trastuzumab-resistant, advanced, HER2-positive breast cancer (PANACEA): a single-arm, multicentre, phase 1b-2 trial. *Lancet Oncol.* **20**, 371–382 (2019).
14. Emens, L. A. et al. 305O - Overall survival (OS) in KATE2, a phase II study of programmed death ligand 1 (PD-L1) inhibitor atezolizumab (atezo)+trastuzumab emtansine (T-DM1) vs placebo (pbo)+T-DM1 in previously treated HER2+ advanced breast cancer (BC). *Ann. Oncol.* **30**, v104 (2019).
15. Loi, S. et al. Prognostic and predictive value of tumor-infiltrating lymphocytes in a phase III randomized adjuvant breast cancer trial in node-positive breast cancer comparing the addition of docetaxel to doxorubicin with doxorubicin-based chemotherapy: BIG 02-98. *JCO* **31**, 860–867 (2013).
16. Denkert, C. et al. Tumour-infiltrating lymphocytes and prognosis in different subtypes of breast cancer: a pooled analysis of 3771 patients treated with neoadjuvant therapy. *Lancet Oncol.* **19**, 40–50 (2018).
17. Samstein, R. M. et al. Tumor mutational load predicts survival after immunotherapy across multiple cancer types. *Nat. Genet* **51**, 202–206 (2019).
18. Elgueta, R. et al. Molecular mechanism and function of CD40/CD40L engagement in the immune system. *Immunol. Rev.* **229**, 152–172 (2009).
19. Vonderheide, R. H. CD40 agonist antibodies in cancer immunotherapy. *Annu. Rev. Med.* **71**, 47–58 (2020).
20. Lin, J. H. et al. Type 1 conventional dendritic cells are systemically dysregulated early in pancreatic carcinogenesis. *J. Exp. Med.* **217**, e20190673 (2020).
21. Ma, D. Y. & Clark, E. A. The role of CD40 and CD154/CD40L in dendritic cells. *Semin. Immunol.* **21**, 265–272 (2009).
22. Van Kooten, C. & Banchereau, J. CD40-CD40 ligand. *J. Leukoc. Biol.* **67**, 2–17 (2000).
23. Zhang, J. Q. et al. Macrophages and CD8+ T cells mediate the antitumor efficacy of combined CD40 ligation and imatinib therapy in gastrointestinal stromal tumors. *Cancer Immunol. Res.* **6**, 434–447 (2018).
24. Schoenberger, S. P., Toes, R. E. M., Van Der Voort, E. I. H., Offringa, R. & Melief, C. J. M. T-cell help for cytotoxic T lymphocytes is mediated by CD40–CD40L interactions. *Nature* **393**, 480–483 (1998).
25. Bennett, S. R. M. et al. Help for cytotoxic-T-cell responses is mediated by CD40 signalling. *Nature* **393**, 478–480 (1998).
26. Morrison, A. H., Diamond, M. S., Hay, C. A., Byrne, K. T. & Vonderheide, R. H. Sufficiency of CD40 activation and immune checkpoint blockade for T cell priming and tumor immunity. *Proc. Natl. Acad. Sci. Usa.* **117**, 8022–8031 (2020).
27. Winograd, R. et al. Induction of T-cell immunity overcomes complete resistance to PD-1 and CTLA-4 blockade and improves survival in pancreatic carcinoma. *Cancer Immunol. Res.* **3**, 399–411 (2015).
28. Bajor, D. L. et al. Long-term outcomes of a phase I study of agonist CD40 antibody and CTLA-4 blockade in patients with metastatic melanoma. *OncoImmunology* **7**, e1468956 (2018).
29. Padrón, L. J. et al. Sotigalimab and/or nivolumab with chemotherapy in first-line metastatic pancreatic cancer: clinical and immunologic analyses from the randomized phase 2 PRINCE trial. *Nat. Med.* **28**, 1167–1177 (2022).

30. O'Hara, M. H. et al. CD40 agonistic monoclonal antibody APX005M (sotigalimab) and chemotherapy, with or without nivolumab, for the treatment of metastatic pancreatic adenocarcinoma: an open-label, multicentre, phase 1b study. *Lancet Oncol.* **22**, 118–131 (2021).
31. Van Laethem, J.-L. et al. Combining CD40 agonist mitazalimab with mFOLFIRINOX in previously untreated metastatic pancreatic ductal adenocarcinoma (OPTIMIZE-1): a single-arm, multicentre phase 1b/2 study. *Lancet Oncol.* **25**, 853–864 (2024).
32. Sheen, M. R. et al. Constitutively activated PI3K accelerates tumor initiation and modifies histopathology of breast cancer. *Oncogenesis* **5**, e267 (2016).
33. Visvader, J. E. Keeping abreast of the mammary epithelial hierarchy and breast tumorigenesis. *Genes Dev.* **23**, 2563–2577 (2009).
34. Le Naour, A., Rossary, A. & Vasson, M. EO771, is it a well-characterized cell line for mouse mammary cancer model? Limit and uncertainty. *Cancer Med.* **9**, 8074–8085 (2020).
35. Le Naour, A. et al. EO771, the first luminal B mammary cancer cell line from C57BL/6 mice. *Cancer Cell Int.* **20**, 328 (2020).
36. Chun, J. & Hartung, H.-P. Mechanism of action of oral fingolimod (FTY720) in multiple sclerosis. *Clin. Neuropharmacol.* **33**, 91–101 (2010).
37. Omland, S. H. et al. Feasibility of intratumoral anti-PD1 as treatment of human basal cell carcinoma: an explorative study with adjuvant ablative fractional laser. *Cancers* **14**, 5815 (2022).
38. Khalil, D. N. et al. In situ vaccination with defined factors overcomes T cell exhaustion in distant tumors. *J. Clin. Investig.* **129**, 3435–3447 (2019).
39. Irenaeus, S. M. M. et al. First-in-human study with intratumoral administration of a CD40 agonistic antibody, ADC-1013, in advanced solid malignancies. *Int. J. Cancer* **145**, 1189–1199 (2019).
40. Beatty, G. L., Li, Y. & Long, K. B. Cancer immunotherapy: activating innate and adaptive immunity through CD40 agonists. *Expert Rev. Anticancer Ther.* **17**, 175–186 (2017).
41. Cardoso, F. et al. Pembrolizumab and chemotherapy in high-risk, early-stage, ER+/HER2- breast cancer: a randomized phase 3 trial. *Nat. Med.* **31**, 442–448 (2025).
42. Loi, S. et al. Neoadjuvant nivolumab and chemotherapy in early estrogen receptor-positive breast cancer: a randomized phase 3 trial. *Nat. Med.* **31**, 433–441 (2025).
43. Bennett, C. N. & Green, J. E. Genomic analyses as a guide to target identification and preclinical testing of mouse models of breast cancer. *Toxicol. Pathol.* **38**, 88–95 (2010).
44. Mohibi, S., Mirza, S., Band, H. & Band, V. Mouse models of estrogen receptor-positive breast cancer. *J. Carcinog.* **10**, 35 (2011).
45. Huffman, A. P., Lin, J. H., Kim, S. I., Byrne, K. T. & Vonderheide, R. H. CCL5 mediates CD40-driven CD4+ T cell tumor infiltration and immunity. *JCI Insight* **5**, e137263 (2020).
46. Tokunaga, R. et al. CXCL9, CXCL10, CXCL11/CXCR3 axis for immune activation—a target for novel cancer therapy. *Cancer Treat. Rev.* **63**, 40–47 (2018).
47. Chow, M. T. et al. Intratumoral activity of the CXCR3 chemokine system is required for the efficacy of anti-PD-1 Therapy. *Immunity* **50**, 1498–1512.e5 (2019).
48. Comerford, I. et al. A myriad of functions and complex regulation of the CCR7/CCL19/CCL21 chemokine axis in the adaptive immune system. *Cytokine Growth Factor Rev.* **24**, 269–283 (2013).
49. Flanagan, K., Moroziewicz, D., Kwak, H., Hörig, H. & Kaufman, H. L. The lymphoid chemokine CCL21 costimulates naive T cell expansion and Th1 polarization of non-regulatory CD4+ T cells. *Cell Immunol.* **231**, 75–84 (2004).
50. French, R. R., Chan, H. T. C., Tutt, A. L. & Glennie, M. J. CD40 antibody evokes a cytotoxic T-cell response that eradicates lymphoma and bypasses T-cell help. *Nat. Med.* **5**, 548–553 (1999).
51. Oh, D. Y. et al. Intratumoral CD4+ T cells mediate anti-tumor cytotoxicity in human bladder cancer. *Cell* **181**, 1612–1625.e13 (2020).
52. Tay, R. E., Richardson, E. K. & Toh, H. C. Revisiting the role of CD4+ T cells in cancer immunotherapy-new insights into old paradigms. *Cancer Gene Ther.* **28**, 5–17 (2021).
53. Osorio, J. C. et al. Fc-optimized CD40 agonistic antibody elicits tertiary lymphoid structure formation and systemic antitumor immunity in metastatic cancer. *Cancer Cell* **43**, 1902–1916.e9 (2025).
54. Perez-Lanzon, M. et al. New hormone receptor-positive breast cancer mouse cell line mimicking the immune microenvironment of anti-PD-1 resistant mammary carcinoma. *J. Immunother. Cancer* **11**, e007117 (2023).
55. Kim, I. S. et al. Immuno-subtyping of breast cancer reveals distinct myeloid cell profiles and immunotherapy resistance mechanisms. *Nat. Cell Biol.* **21**, 1113–1126 (2019).
56. Cotrim, C. Z. et al. Estrogen receptor beta growth-inhibitory effects are repressed through activation of MAPK and PI3K signalling in mammary epithelial and breast cancer cells. *Oncogene* **32**, 2390–2402 (2013).


## Acknowledgements

Acknowledgments to Jose Conejo-Garcia, the University of Pennsylvania core services: Penn Vet Comparative Pathology Core, Molecular Pathology and Imaging Core (Center for Molecular Studies in Digestive and Liver Diseases, P30DK050306), and Penn Cytomics Core. Early-stage Surgeon Scientist Program to J.Q.Z. (P30CA016520-46), Breast Cancer Research Foundation to R.H.V. (BCRF-24-167), University of Pennsylvania Department of Surgery Pilot Grant to J.Q.Z., Abramson Cancer Center Pilot Grant to J.Q.Z., Thomas B. and Jeannette E. Laws McCabe Fund to J.Q.Z. (Funders played no role in study design, data collection, analysis, and interpretation of data, or writing of this manuscript.).

## Author contributions

J.Q.Z., C.L., O.L., V.M., N.J., C.R.F., and X.H. performed experiments, designed methodology, and performed data analysis. N.J. and X.H. performed computational analysis. J.Q.Z., N.M., S.Z., R.P.D., and R.H.V. were involved in conceptualization and manuscript preparation. All authors were involved in data interpretation, manuscript review and editing.

## Competing interests

Dr. Vonderheide has received consulting fees from BMS, EMD Serono, Grey Wolf Therapeutics and Crossbow Therapeutics, research funding from Revolution Medicines, is an inventor on patents relating to cancer cellular immunotherapy, cancer vaccines, and KRAS immune epitopes, and receives royalties from Children's Hospital Boston for a licensed research-only monoclonal antibody, but declares no non-financial competing interests. All other authors declare no financial or non-financial competing interests.

## Additional information

**Supplementary information** The online version contains supplementary material available at https://doi.org/10.1038/s41523-025-00889-7.

**Correspondence** and requests for materials should be addressed to Jennifer Q. Zhang.